

# Concentration of Vacancies at Metal Oxide Surfaces: Case Study of MgO (100)

Norina A. Richter,<sup>1</sup> Sabrina Sicolo,<sup>2</sup> Sergey V. Levchenko,<sup>1</sup> Joachim Sauer,<sup>2</sup> and Matthias Scheffler<sup>1</sup>

<sup>1</sup>*Fritz-Haber-Institut der Max-Planck-Gesellschaft, Faradayweg 4-6, 14195 Berlin, Germany*

<sup>2</sup>*Institut für Chemie, Humboldt Universität zu Berlin, Unter den Linden 6, 10099 Berlin, Germany*

We investigate effects of doping on formation energy and concentration of oxygen vacancies at a metal oxide surface, using MgO (100) as an example. Our approach employs density-functional theory, where the performance of the exchange-correlation functional is carefully analyzed, and the functional is chosen according to a fundamental condition on DFT ionization energies. The approach is further validated by CCSD(T) calculations for embedded clusters. We demonstrate that the concentration of oxygen vacancies at a doped oxide surface is largely determined by formation of a macroscopically extended space charge region.

PACS numbers: 61.72.Bb, 61.72.jd, 68.55.Ln, 68.47.Gh, 68.35.-p

Metal oxides are key materials for many technological applications. For example, MgO is used as a catalyst for methane oxidation, TiO<sub>2</sub> plays an important role as a photocatalyst, and RuO<sub>2</sub> catalyzes the oxidation of carbon monoxide. It is generally accepted that intrinsic point defects, in particular oxygen vacancies (also called F or color centers), play a decisive role in catalysis at oxide surfaces [1–4], but significant controversy exists regarding their formation energy, concentration, and charge state. In this paper we study these issues for MgO bulk and the MgO (100) surface in contact with an O<sub>2</sub> gas phase at realistic temperature and pressure. Furthermore, we consider that realistic metal oxides are typically doped, either intentionally or unintentionally. Although the experimental band gap of MgO is 7.8 eV [5], realistic samples are typically neither clear transparent nor insulating. Defects such as intrinsic point defects, impurities, and defect complexes can give rise to electron or hole conductivity [1, 6, 7]. In this paper, we neglect defect complexes (e.g. dopant plus vacancy). Thus, for our study the role of dopants is to create a Fermi level, *i.e.* a reservoir for electrons and holes. This is termed “the global effect of doping”. We focus our discussion on *p*-type MgO, since it exhibits intriguing catalytic properties [1, 8, 9]. Still our theoretical model covers also *n*-type material, where the concentration of F centers is very low. Our main finding is that for *p*-type samples, surface O vacancies get doubly positively charged which lowers their formation energy and results in a significant defect concentration. In fact, the free energy of formation in thermodynamic equilibrium is negative under typical catalytic temperatures and pressures. We show that the limiting factor to formation of surface oxygen vacancies is the formation of a space charge region (Fig. 1). Although well-known for doped semiconductor surfaces, the effect of space charge and band bending on the concentration of surface defects has not been discussed so far.

The values of calculated defect energy levels and total energies are sensitive to the employed treatment of exchange and correlation (xc) of the many-electron system. Therefore, special attention is given below to this aspect:

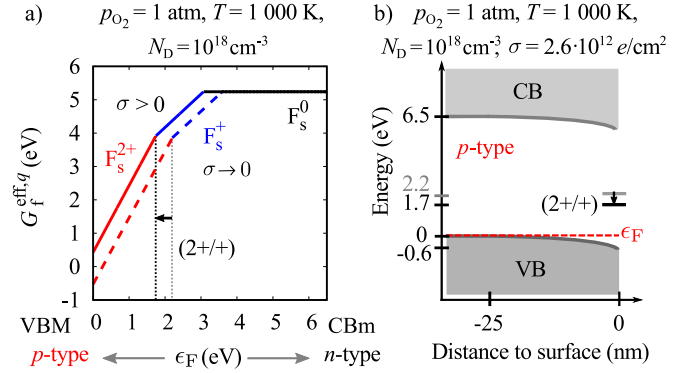


FIG. 1. a) Calculated Gibbs free energies of formation  $G_f^{\text{eff},q}$  (see text) of F centers at MgO (100) for  $T = 1\,000\text{ K}$  and normal pressure of oxygen, as a function of Fermi energy,  $\epsilon_F$ , between valence-band maximum, VBM, and conduction band minimum, CBm. Realistic dopant concentration  $N_D=10^{18}\text{ cm}^{-3}$  and surface charge density  $\sigma = 2.6 \cdot 10^{12} \frac{e}{\text{cm}^2}$  (solid lines) and the dilute limit  $\sigma \rightarrow 0$  (dashed lines) are shown. b) In *p*-type MgO ( $\epsilon_F=\text{VBM}$ ) under realistic conditions, band bending, due to formation of a space charge region, limits the formation of surface  $F_s^{2+}$  centers.

Our approach is to determine the best xc functional of the HSE family by the condition that the ionization potentials obtained with the optimized (opt-) HSE functional agree with the results of a  $G_0W_0$  calculation. In exact DFT such condition must be fulfilled exactly [10]. However, due to the limited flexibility of the HSE family of functionals, which range from the PBE [11] generalized gradient approximation via the HSE06 [12] hybrid functional to the PBE0 [13] hybrid functional, our approach is obviously not exact, but it is “the best compromise”. In terms of the HSE [14] exchange and range-separation parameters ( $\alpha, \omega$ ), the three mentioned functionals correspond to (0, arbitrary), (0.25, 0.11 bohr<sup>-1</sup>), (0.25, 0). Our approach is validated for neutral, embedded  $\text{Mg}_x\text{O}_y$  clusters using the CCSD(T) method.

In this work, we use the all-electron FHI-aims code [22] for the periodic structures (bulk and surfaces) and some embedded cluster calculations. FHI-aims employs atom-

centered numeric basis functions and various xc functionals as well as the *GW* approach. The basis set and numerical grids are of high quality as defined by the *tight* [22] settings. For all periodic surface models full atomic relaxation is calculated using PBE at the PBE bulk lattice parameter (4.258 Å). HSE calculations are performed at these geometries, since using HSE geometries for two smallest unit cells considered results in negligible changes in the calculated formation energies. Vibrational energy  $\Delta F_{\text{vib}}^q(T)$  and vdW contributions to the formation energies were analyzed as well [23], but found to be insignificant for this study.

Furthermore, we employ the TURBOMOLE program package [24] for various embedded clusters using different xc functionals and CCSD(T). Triple-zeta valence plus polarization basis sets  $[5s3p2d1f] / [5s4p3d]$  are used [25]. For the CCSD(T) computations we correlate also electrons in the Mg 2*s* and 2*p* shells, using core-valence correlation consistent basis sets, cc-pCVXZ (X = D, T, Q). On the  $\text{O}^{2-}$  ions we use the aug-cc-pVXZ basis sets [26]. In both CCSD(T) and DFT calculations, the basis set superposition error was evaluated following the Boys-Bernardi counterpoise correction [27]. MgO clusters are embedded in a periodic point charge array using the periodic electrostatic embedded cluster model [28] in TURBOMOLE and a converged finite set of point charges in FHI-aims. (See supplemental information (SI) at [URL will be inserted by publisher] for more details.)

To minimize non-physical polarization of peripheral oxygen anions by the embedding point charges, pseudopotentials were added to the first shell of embedding  $\text{Mg}^{2+}$  cations (all-electron Hay&Wadt effective core potentials [29] in TURBOMOLE, and Troullier-Martins-type norm-conserving non-local pseudopotentials [30, 31] in FHI-aims). The PBE lattice constant has been used for the embedded clusters. Apart from the outermost frozen shell of atoms, full relaxation is allowed for in the cluster calculations, except for the CCSD(T) and *GW* calculations and respective DFT values.

In realistic samples defects may get charged due to electron transfer between the dopant-induced Fermi level and the defect states [15]. The neutral oxygen vacancy in MgO bulk and at the MgO (100) surface has an energy level deep in the band gap. This state has *s*-like symmetry at the defect site, and is fully occupied by two electrons. Thus, a singly and even a doubly charged vacancy is possible. In FHI-aims this situation can be modeled in two ways: either by adding a constant charge density to the density entering the Hartree term, or by slightly modifying the nuclear charges of the atoms in the unit cell. Either concept enables us to describe a charged defect while the supercell is kept neutral. The “constant density approach” is the standard treatment in other periodic codes. For surfaces, where much of the supercell corresponds to vacuum, this approach is obviously unphysical, although it can be partially remedied

by *a posteriori* correction schemes [16]. The other treatment corresponds to the virtual-crystal approximation (VCA) [17, 18] of a crystal with dopants. We change the nuclear number of all Mg atoms in the supercell by  $\Delta Z_{\text{Mg}} = -q/N_{\text{Mg}}$ , where  $q$  is the charge of the oxygen vacancy (+1 or +2), and  $N_{\text{Mg}}$  is the number of Mg atoms in the supercell. This means that 1 or 2 electrons are transferred to the VBM, which is the Fermi level in the virtual crystal. Once known for one particular Fermi level, the O vacancy formation energy can be trivially calculated for an arbitrary Fermi level (see Eq. 1).

When removing atoms from the bulk or from the surface of a material, we need to consider also a reservoir to which the atoms are brought [19, 20]. We assume a gas phase of  $\text{O}_2$  molecules which is characterized by an oxygen chemical potential,  $\mu_{\text{O}}(T, p)$  [20]. For an isolated oxygen vacancy, the Gibbs free energy of formation is:

$$G_{\text{f}}^q = E_{\text{vac}}^q - E_{\text{host}} + \mu_{\text{O}} + q\epsilon_{\text{F}} + \Delta F_{\text{vib}}^q(T). \quad (1)$$

Here,  $E_{\text{vac}}^q$  and  $E_{\text{host}}$  are DFT total energies of defected and undefected systems, respectively,  $\Delta F_{\text{vib}}^q$  is the change in vibrational Helmholtz free energy of the crystal upon defect formation,  $q$  is the defect charge, and  $\epsilon_{\text{F}}$  is the Fermi energy. The oxygen chemical potential is

$$\mu_{\text{O}} = E_{\text{O}} - \frac{1}{2}E_{\text{O}_2}^{\text{bind}} + \Delta\mu_{\text{O}}, \quad (2)$$

where  $\Delta\mu_{\text{O}}$  contains the vibrational and other *T*- and *p*-dependent terms [20]. We use the experimental binding energy without zero point energies  $E_{\text{O}_2}^{\text{bind}} = 5.22$  eV [21] to reduce artifacts originating from the generalized gradient approximations for the binding of the  $\text{O}_2$  molecule, but the calculated total energy of the free atom,  $E_{\text{O}}$ , is calculated with the corresponding electronic-structure approach.  $\Delta\mu_{\text{O}} = 0$  defines the oxygen-rich limit.

First, we address formation energies for isolated vacancies in the bulk,  $G_{\text{f}}^{\text{bulk},q}$ . We extrapolate our DFT formation energies to the dilute limit using Taylor expansion in terms of reciprocal supercell lattice constant. In agreement with related work [32], we find that the charge-transition levels (2+/+) and (+/0), as well as formation energies  $G_{\text{f}}^{\text{bulk},q}$ , are almost independent on the xc functional within the HSE family, when referenced to the vacuum level. However, given the more realistic situation of *p*-type material, where  $\epsilon_{\text{F}}$  is at VBM,  $G_{\text{f}}^{\text{bulk},q}$  does depend strongly on the choice of HSE parameters ( $\alpha$ ,  $\omega$ ) for  $q \neq 0$ . The formation energy of the neutral defect is insensitive to the functional. We find that the main error in charged defect formation energies is the error in the VBM position with respect to vacuum (also pointed out in [33]). For fixed  $\omega$  the formation energies depend practically linearly on the exchange parameter  $\alpha$ , which can be traced back to a linear dependence of VBM with respect to vacuum on  $\alpha$ .

Next, we identify the optimal xc functional to describe the formation energies of F centers in MgO. The ion-

ization potential at a fixed defect geometry for a given functional HSE( $\alpha$ ,  $\omega$ ) is

$$I_{\Delta\text{SCF}}^{q \rightarrow q+1} = E_{\text{vac}}^{q+1} + \epsilon_F - E_{\text{vac}}^q, \quad (3)$$

where both  $E_{\text{vac}}^q$  and  $E_{\text{vac}}^{q+1}$  are extrapolated to the dilute limit. For  $\epsilon_F = \text{VBM}$ ,  $I_{\Delta\text{SCF}}^{q \rightarrow q+1}$  depends on ( $\alpha$ ,  $\omega$ ). In exact DFT the Kohn-Sham highest occupied orbital (HOMO) does not change with occupation and agrees with the ionization energy. A more practical request is that the HOMO, calculated by  $G_0W_0$  on top of the HSE electronic ground state, should agree with the HSE ionization energy

$$I_{G_0W_0}^{q \rightarrow q+1} = \epsilon_F - \epsilon_{\text{HOMO}}^{G_0W_0} \stackrel{!}{=} I_{\Delta\text{SCF}, \text{opt-HSE}}^{q \rightarrow q+1}, \quad (4)$$

identifying what we call the optimized HSE functional, opt-HSE that correctly describes the charge excitation of the defect.

We determine the opt-HSE functional for fixed  $\omega = 0.11 \text{ bohr}^{-1}$ . The ionization energy  $I^{0 \rightarrow +}$  for  $\epsilon_F$  at VBM at  $F^0$  geometry is calculated for an embedded  $\text{Mg}_6\text{O}_9$  cluster model using FHI-aims. The Fermi level  $\epsilon_F$  is obtained as  $\text{VBM} = E_{\text{host}}^{+1} - E_{\text{host}}$  using HSE, and from the HOMO of the host system in the corresponding  $G_0W_0$ @HSE calculations. The ionization potential shows a near-linear dependence on the exchange parameter  $\alpha$  (Fig. 2) for both  $\Delta\text{SCF}$  and  $GW$  method. The intersection of the two linear fits is at  $\alpha=0.27$ , very close to HSE06 with parameter set ( $\alpha=0.25$ ,  $\omega = 0.11 \text{ bohr}^{-1}$ ). We therefore use HSE06 as our opt-HSE functional that correctly describes the charge excitation of the defect. The difference in formation energies with  $\alpha=0.25$  instead of  $\alpha=0.27$  is negligible for  $F^0$ , less than 0.1 eV for  $F^{2+}$ , and less than 0.2 eV for  $F^{2+}$ .

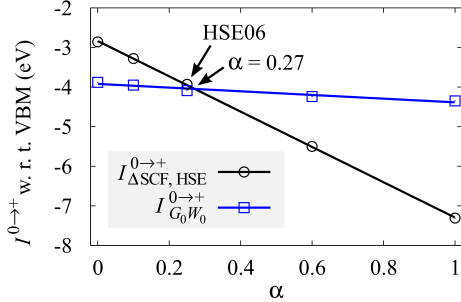


FIG. 2. Ionization potential at  $F^0$  geometry calculated for an  $\text{Mg}_6\text{O}_9$  embedded cluster by  $\Delta\text{SCF}$  with HSE xc functionals (black symbols) and from the HOMO of a  $G_0W_0$ @HSE calculation (blue symbols). The screening parameter is  $\omega = 0.11 \text{ bohr}^{-1}$ . Solid lines show linear fits to the ionization energies as a function of exchange parameter  $\alpha$ .

We perform a validation for the  $F^0$  formation energy using an unrelaxed  $\text{Mg}_6\text{O}_9$  cluster model and the CCSD(T) method. This results in a correction

$\Delta\text{CCSD(T)}$  of the DFT formation energies of  $-0.09 \text{ eV}$  for PBE,  $0.07 \text{ eV}$  for PBE0, and  $-0.28 \text{ eV}$  for B3LYP. Adding these corrections to the DFT formation energies ( $\Delta\mu_{\text{O}} = 0$ ) for a converged cluster size  $\text{Mg}_{16}\text{O}_{19}$  yields DFT+ $\Delta\text{CCSD(T)}$  results of 6.85, 6.88 and 6.89 eV, respectively. These numbers are in good agreement with the HSE06  $F^0$  formation energies 7.04 eV and 7.05 eV obtained from the same converged embedded cluster and periodic calculations, respectively, using FHI-aims.

Thus, HSE06 is the opt-HSE functional in accordance with  $GW$  as well as coupled-cluster results. Our results show that the experimental value for the bulk  $F^0$  center formation enthalpy in  $\text{MgO}$  of 9.29 eV with respect to the  $\text{O}_2$  molecule [34, 35] is a significant overestimate. A likely reason is that thermodynamic equilibrium has not been reached in this experiment.

We are now on solid grounds to provide an accurate estimate of  $G_{\text{f}}^{\text{surf}, q}$  for isolated oxygen vacancies at the surface using our periodic model and the HSE06 xc functional.  $F_{\text{s}}^0$ ,  $F_{\text{s}}^+$ , and  $F_{\text{s}}^{2+}$  formation energies in the dilute limit are 6.34 eV, 2.76 eV, and 0.55 eV, respectively, for  $\Delta\mu_{\text{O}} = 0$  and  $\epsilon_F$  at VBM. For more realistic conditions, the formation energies are lower, as shown in Fig. 1a).  $E_{\text{f}}^{\text{surf}, 0}$  obtained with the CCSD(T) correction method, is, as for the bulk, in good agreement with the HSE06 value. The corrections  $\Delta\text{CCSD(T)}$  to the DFT formation energies, calculated with an unrelaxed  $\text{Mg}_5\text{O}_5$  model, are  $-0.26 \text{ eV}$  for PBE,  $-0.01 \text{ eV}$  for PBE0, and  $-0.28 \text{ eV}$  for B3LYP, yielding DFT+ $\Delta\text{CCSD(T)}$  values of 6.23, 6.25 and 6.33 eV, respectively.

Formation energies of *neutral* O vacancies depend weakly on their concentration (up to approx. 3% for bulk and 12% for surface defects in  $\text{MgO}$ ). On the contrary, due to the slow decay of Coulomb interaction with distance, the formation energy of *charged* defects will strongly depend on their concentration, as well as the distribution of the compensating charge. Thus, concentration of dopants  $N_{\text{D}}$  and their distribution (doping profile) should have a strong global effect on the defect formation energies. The equilibrium concentrations  $\eta_q$  of oxygen vacancies in three different charge states ( $q = 0 - 2$ ) are determined by the minimum of the total free energy  $G$  of the system with interacting defects:

$$\frac{\partial G}{\partial \eta_q} = G_{\text{f}}^{\text{eff}, q}(\eta_0, \eta_1, \eta_2) - T \frac{\partial s_{\text{conf}}(\eta_0, \eta_1, \eta_2)}{\partial \eta_q} = 0, \quad (5)$$

where

$$G_{\text{f}}^{\text{eff}, q}(\eta_0, \eta_1, \eta_2) = \frac{\partial}{\partial \eta_q} \sum_{r=0}^2 \eta_r G_{\text{f}}^r(\eta_0, \eta_1, \eta_2) \quad (6)$$

is an effective formation energy of a vacancy in charge state  $q$  in the presence of other vacancies. The configurational entropy  $s_{\text{conf}}$  accounts for energetically degenerate arrangements of the defects (see SI).

Surface defects are charged by accommodating charge carriers from the bulk. This results in depletion of the charge carriers and creation of a space charge layer in the subsurface region. The resulting electrostatic potential causes band bending and prevents more charges from the bulk to reach the surface, increasing the energy cost per defect. As a result, there are two leading electrostatic contributions to the formation energy of charged defects: (i) attraction to the compensating charge, and (ii) band bending. The first contribution reduces the formation energy, while the second contribution increases it. The thickness of the space charge layer,  $z^{\text{SC}}$ , depends on the doping profile, and may be limited by the thickness of the material. We consider the case of uniformly distributed dopants and unconstrained  $z^{\text{SC}}$ , but the discussion can be straightforwardly generalized to the more complex situations. To stay focussed on electrostatic effects, we also do not consider a possible  $(T, p)$  dependence of the bulk charge carrier density  $N_{e/h}^{\text{bulk}}$ , i.e.  $N_{e/h}^{\text{bulk}} \equiv N_D$  is a constant external parameter.

The dependence of  $G_f^{\text{surf},q}$  on the surface charge density  $\sigma$  is calculated as follows. First, we calculate formation energies  $G_f^{\text{surf},q}(\sigma, z^{\text{SC}})$  at a fixed  $z^{\text{SC}}$ , equal to the slab thickness  $d$ , using VCA (see SI). The calculated formation energies include both electrostatic effects mentioned above. The actual  $z^{\text{SC}}$  is determined by  $N_D$  as follows:

$$z^{\text{SC}} = \frac{\sigma}{eN_D}, \quad (7)$$

where  $e$  is the absolute value of the electron charge. The formation energy as a function of  $\sigma$  and  $z^{\text{SC}}$  is

$$G_f^{\text{surf},q}(\sigma) = G_f^{\text{surf},q}(\sigma, d) - qE^{\text{SC}}(\sigma, d) + qE^{\text{SC}}(\sigma, z^{\text{SC}}), \quad (8)$$

where

$$E^{\text{SC}}(\sigma, z^{\text{SC}}) = \frac{e\sigma}{6\epsilon_r\epsilon_0}z^{\text{SC}} \quad (9)$$

is the classic expression for the energy of the space charge region formation at a semiconductor surface. The temperature dependence of  $z^{\text{SC}}$  and  $E^{\text{SC}}(\sigma, z^{\text{SC}})$  at fixed  $\sigma$  is neglected. The meaning of the last two terms in Eq. 8 is to replace the band bending contribution to the formation energy calculated for  $z^{\text{SC}} = d$  with the one obtained for the actual  $z^{\text{SC}}$  from Eq. 7. The remaining dependence on  $\sigma$  after subtracting  $qE^{\text{SC}}(\sigma, d)$  from  $G_f^{\text{surf},q}(\sigma, d)$  is due to the electrostatic attraction between the defect and the compensating charge.

We can now calculate the equilibrium concentration of O vacancies at a  $p$ -doped MgO (100) surface, using Eq. 5.  $G_f^{\text{eff},q}(\sigma)$  is calculated from Eq. 6 with  $\sigma = e\eta_1 + 2e\eta_2$ . The concentrations of  $F_s^0$  and  $F_s^+$  are found to be negligible at realistic  $T$ ,  $p_{\text{O}_2}$ , and  $N_D$ . The  $F_s^{2+}$  concentration  $\eta_2$  and corresponding  $z^{\text{SC}}$  as functions of  $N_D$  are shown in Fig. 3 for different temperatures and  $p_{\text{O}_2} = 1$  atm. Although the  $F_s^{2+}$  Gibbs free energy of formation at  $\sigma \rightarrow 0$

is small or even negative at elevated temperatures, the equilibrium defect concentration does not exceed  $\sim 0.5\%$  at  $N_D \leq 10^{18} \text{ cm}^{-3}$ . Thus, space charge layer formation can be a mechanism by which wide-band-gap semiconductor surfaces remain stable at high temperatures. The

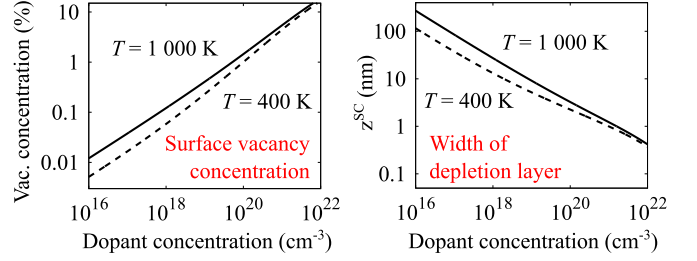


FIG. 3. *Left:*  $F_s^{2+}$  concentration as a function of dopant concentration  $N_D$  for two different temperatures and oxygen partial pressure of 1 atm. *Right:* Dependence of the space charge depth  $z^{\text{SC}}$  on  $N_D$ .

band bending profile for  $\epsilon_F = \text{VBM}$  at  $T = 1000$  K for  $p_{\text{O}_2} = 1$  atm and  $N_D = 10^{18} \text{ cm}^{-3}$  is shown in Fig. 1b). Under these conditions the bulk bands bend downwards by 0.6 eV, and the  $(2+/+)$  charge transition level is lowered from 2.2 eV to 1.7 eV above the Fermi level. At  $T = 1000$  K and  $p_{\text{O}_2} = 1$  atm, the contribution of the electrostatic attraction term is small for small  $N_D$ , but becomes comparable to the formation energy in the dilute limit for  $N_D > 10^{18} \text{ cm}^{-3}$ .

We have presented a methodology for calculating charged defect formation energies and concentrations at surfaces, taking into account electrostatic effects due to charge transfer between surface and bulk. Doped material has been simulated using the VCA, and an optimal DFT functional has been identified by validation with coupled-cluster and  $GW$  methods. Our analysis shows that the concentration of  $F_s^{2+}$  centers at the (100) terrace of  $p$ -type MgO can be as high as 1% at realistic conditions, while relative  $F_s^+$  and  $F_s^0$  concentrations are negligible. We demonstrate that the formation of charged vacancies creates a localized, although macroscopically extended, space charge region. This decreases charge transition levels with respect to Fermi level at the surface, raising the formation energy by up to 1 eV and, therefore, limiting the defect concentration. We conclude that electrostatic effects can largely control oxygen vacancy formation at the surface of metal oxides. Experimental information on doping profiles may provide new insights on catalytic activity of doped oxide surfaces.

This collaboration was financially supported by the cluster of excellence UniCat. N. A. R. acknowledges financial support from the International Max Planck Research School "Complex Surfaces in Materials Science". S. V. L. acknowledges financial support from the Alexander von Humboldt-Foundation.



- 
- [1] I. Balint and K.-i. Aika, Appl. Surf. Sci. **173**, 296 (2001)
  - [2] E. Wahlström, E. K. Vestergaard, R. Schaub, A. Ronnau, M. Vestergaard, E. Laegsgaard, I. Stensgaard, and F. Besenbacher, Science **303**, 511 (2004)
  - [3] Z. Yan, S. Chinta, A. A. Mohamed, J. P. Fackler, and D. W. Goodman, J. Am. Chem. Soc. **127**, 1604 (2005)
  - [4] D. O. Scanlon, A. Walsh, B. J. Morgan, and G. W. Watson, e-J. Surf. Sci. Nanotech. **7**, 395 (2009)
  - [5] R. C. Whited and W. C. Walker, Phys. Rev. Lett. **22**, 1428 (1969)
  - [6] S. P. Mitoff, J. Chem. Phys. **31**, 1261 (1959)
  - [7] N. I. Hadi, J. Earth Sci. Climat. Change **03** (2012)
  - [8] J.-L. Dubois and C. J. Cameron, Appl. Catal. **67**, 49 (1990)
  - [9] S. Arndt, G. Laugel, S. Levchenko, R. Horn, M. Baerns, M. Scheffler, R. Schlögl, and R. Schomäcker, Cat. Rev. **53**, 424 (2011)
  - [10] M. Levy and A. Görling, Phys. Rev. B **53**, 969 (1996)
  - [11] J. P. Perdew, K. Burke, and M. Ernzerhof, Phys. Rev. Lett. **77**, 3865 (1996)
  - [12] A. V. Krukau, O. A. Vydrov, A. F. Izmaylov, and G. E. Scuseria, J. Chem. Phys. **125**, 224106 (2006)
  - [13] J. P. Perdew, M. Ernzerhof, and K. Burke, J. Chem. Phys. **105** (1996)
  - [14] J. Heyd, G. E. Scuseria, and M. Ernzerhof, J. Chem. Phys. **118**, 8207 (2003)
  - [15] C. Weinert and M. Scheffler, in *Defects in Semiconductors, Mater. Sci. Forum*, Vol. 10–12, edited by H. J. Bardeleben (Trans Tech Publications, Ltd., Aedermannsdorf, Switzerland, 1986) p. 25
  - [16] H.-P. Komsa and A. Pasquarello, Phys. Rev. Lett. **110**, 095505 (2013)
  - [17] L. Vegard, Z. Phys. **5**, 17 (1921)
  - [18] M. Scheffler, Physica B+C **146**, 176 (1987)
  - [19] M. Scheffler and J. Dabrowski, Philos. Mag. A **58**, 107 (1988)
  - [20] K. Reuter, C. Stampfl, and M. Scheffler, in *Handbook of Materials Modeling*, Vol. 1 (2005) pp. 149–194
  - [21] D. Feller and K. A. Peterson, J. Chem. Phys. **110**, 8384 (1999)
  - [22] V. Blum, R. Gehrke, F. Hanke, P. Havu, V. Havu, X. Ren, K. Reuter, and M. Scheffler, Comput. Phys. Commun. **180**, 2175 (2009), <https://aimsclub.fhi-berlin.mpg.de>
  - [23] N. A. Richter, S. V. Levchenko, and M. Scheffler, to be published
  - [24] TURBOMOLE V6.3 2011, a development of University of Karlsruhe and Forschungszentrum Karlsruhe GmbH, 1989-2007, TURBOMOLE GmbH, since 2007
  - [25] F. Weigend and R. Ahlrichs, PCCP **7**, 3297 (2005)
  - [26] T. H. Dunning Jr, J. Chem. Phys., 1007(1989)
  - [27] S. F. Boys and F. B. Bernardi, Mol. Phys., 553(1970)
  - [28] A. M. Burow, M. Sierka, J. Döbler, and J. Sauer, J. Chem. Phys. **130**, 174710 (2009)
  - [29] P. J. Hay and W. R. Wadt, J. Chem. Phys. **82**, 270 (1985)
  - [30] L. Kleinman and D. M. Bylander, Phys. Rev. Lett. **48**, 1425 (1982)
  - [31] M. Fuchs and M. Scheffler, Comput. Phys. Commun. **119**, 67 (1999)
  - [32] R. Ramprasad, H. Zhu, P. Rinke, and M. Scheffler, Phys. Rev. Lett. **108**, 066404 (2012)
  - [33] D. West, Y. Y. Sun, and S. B. Zhang, Appl. Phys. Lett. **101**, 082105 (2012)
  - [34] L. A. Kappers, R. L. Kroes, and E. B. Hensley, Phys. Rev. B **1**, 4151 (1970)
  - [35] Weast, *CRC Handbook of Chemistry and Physics 61st Edition*, 61st ed. (CRC Press, 1980)

# Concentration of Vacancies at Metal-Oxide Surfaces: Case Study of MgO (100)

## – Supplemental information –

N. A. Richter,<sup>1</sup> S. Siculo,<sup>2</sup> S. V. Levchenko,<sup>1</sup> J. Sauer,<sup>2</sup> M. Scheffler<sup>1</sup>

<sup>1</sup>*Fritz-Haber-Institut der Max-Planck-Gesellschaft, Faradayweg 4-6, 14195 Berlin, Germany*

<sup>2</sup>*Institut für Chemie, Humboldt Universität zu Berlin, Unter den Linden 6, 10099 Berlin, Germany*

### 1 Calculations on embedded cluster models

Formation energies for F centers at the MgO (100) terrace and at low coordinated sites were calculated with different methods, some of them using FHI-aims and TURBOMOLE to insure consistency of the two codes.

#### 1.1 Cluster definition

Fig. S1 shows the cluster models that were employed for the DFT calculations of formation energies for defects at different configurational sites of the MgO (100) surface. All the clusters are embedded in a periodic array of point charges at the optimized PBE (pbc) cell parameter. For the surface models the positions of the point charges coincide with the coordinates of a relaxed defect-free 5-layer slab.

The CCSD(T) computations for the neutral oxygen vacancy in the bulk and at the MgO (100) terrace were performed using the embedded cluster models shown in Fig. S2. While all other embedded cluster calculations were performed with TURBOMOLE, this model was also used for FHI-aims calculations at DFT level.

#### 1.2 Defect formation energies as a function of cluster size

To incorporate long-range polarization effects we extrapolate the formation energies of the charged surface defects according to

$$G_f^q(n) = G_f^q(n \rightarrow \infty) + a \left(\frac{1}{n}\right)^{\frac{1}{3}}, \quad (1.1)$$

where  $n$  is the number of ions in the cluster [1]. For all cluster calculations the Fermi level is at VBM and the chemical potential of oxygen is  $\mu_O = 1/2 E_{O_2}$ . Since we do not relax all ions in the cluster, we use separate extrapolations for the vertical formation energy,  $n = n_{\text{total}}$ , and for the relaxation energy,  $n = n_{\text{relax}}$ . The formation energy of the relaxed defect is the sum of the vertical formation energy and the relaxation energy:

$$G_f^q = G_{f,\text{vert}}^q + E_{\text{relax}}^q. \quad (1.2)$$

With regard to the formation energies of the charged defects, we find that including long-range polarization effects is an important requirement for an accurate description, as mentioned by Sushko et al. [2]. The unrelaxed (vertical) formation energies and relaxation energies for F centers at MgO (100) have been obtained from a series of clusters including  $\text{Mg}_9\text{O}_9$  ( $3 \times 3 \times 2$  ions),  $\text{Mg}_{25}\text{O}_{25}$  ( $5 \times 5 \times 2$  ions) and  $\text{Mg}_{50}\text{O}_{50}$  ( $5 \times 5 \times 4$  ions). In Table S1 the vertical formation energies and relaxation energies obtained with PBE are summarized. The corresponding extrapolations are shown in Fig. S3.

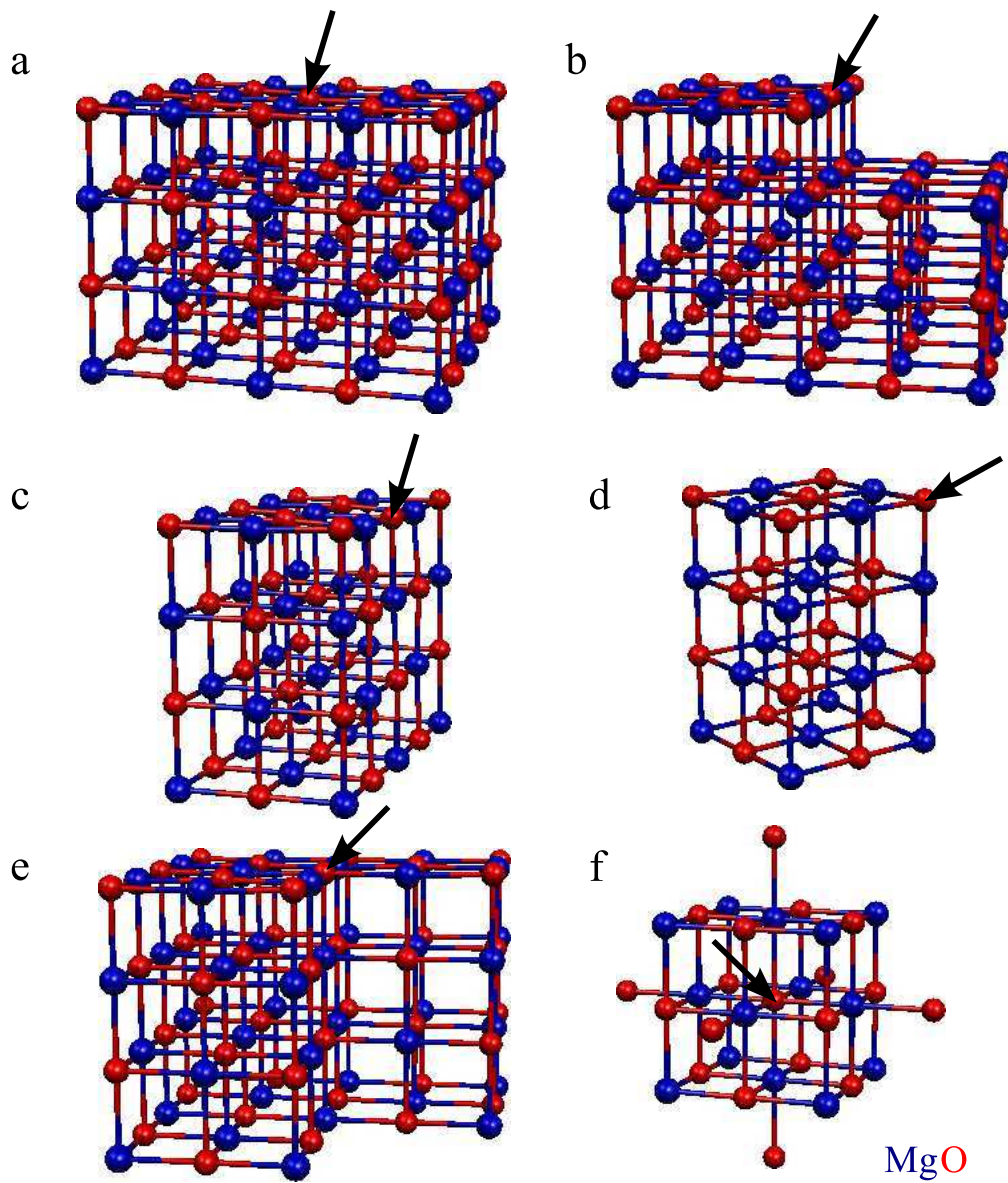


Figure S1: Cluster models for different sites: a) terrace ( $\text{Mg}_{50}\text{O}_{50}$ ), b) step ( $\text{Mg}_{45}\text{O}_{45}$ ), c) edge ( $\text{Mg}_{30}\text{O}_{30}$ ), d) corner ( $\text{Mg}_{18}\text{O}_{18}$ ), e) reverse corner ( $\text{Mg}_{42}\text{O}_{42}$ ) and f) bulk ( $\text{Mg}_{14}\text{O}_{19}$ ). The arrows indicate which atom was removed to form the defect.

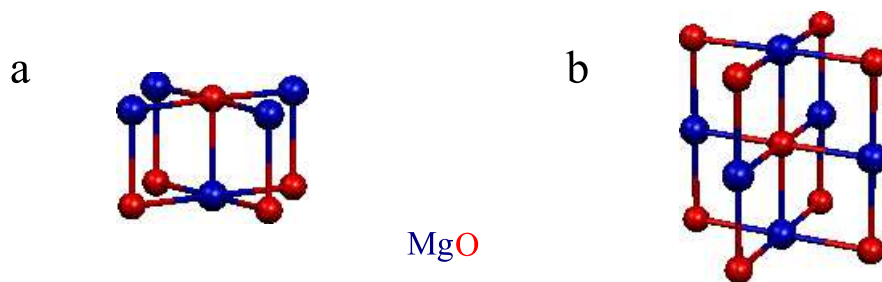


Figure S2: Cluster models for terrace ( $\text{Mg}_5\text{O}_5$ , a) and bulk ( $\text{Mg}_6\text{O}_9$ , b) used for comparison of DFT and CCSD(T) calculations.

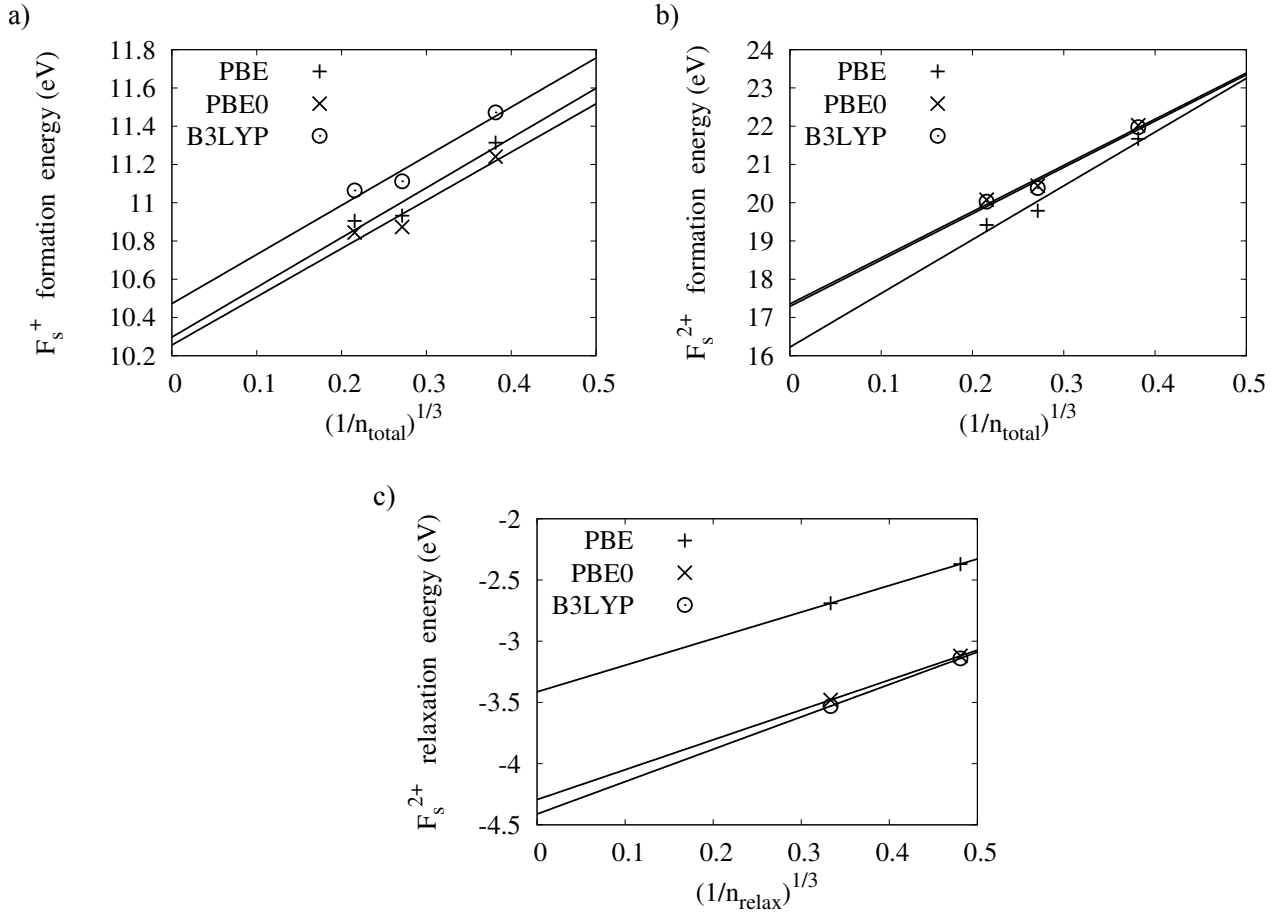


Figure S3: Extrapolated vertical formation energies for  $F_s^+$  (a) and for  $F_s^{2+}$  (b), and extrapolated relaxation energy for  $F_s^{2+}$  (c), calculated with PBE, PBE0 and B3LYP.

Table S1: Vertical formation energies, relaxation energies, and formation energies including relaxation as obtained from embedded cluster and supercell calculations (PBE), all in eV.

Type of defect	Model	$G_{f,\text{vert}}^q$	$E_{\text{relax}}^q$	$G_f^q$
$F_s^+$	Supercell	10.71	-1.21	9.50
$F_s^+$	Emb. cluster	10.28	-0.81	9.47
$F_s^{2+}$	Supercell	16.54	-3.23	13.31
$F_s^{2+}$	Emb. cluster	16.21	-3.35	12.86



### 1.3 Comparison between DFT and CCSD(T) embedded cluster calculations for the neutral oxygen vacancy

Table S2 summarizes the vertical formation energies for a neutral  $F^0$  center at the (100) terrace ( $Mg_5O_5$ ) and in MgO bulk ( $Mg_6O_9$ ). For consistency, bulk defect formation energies calculated with FHI-aims using a *tight*, *Tier 3* basis are shown, too. Also DFT formation energies using larger clusters are reported to show that the small clusters are already converged with respect to cluster size within 0.1 eV in vertical formation energy for the bulk defect and within 0.23 eV for the surface defect. In the main part of the paper we report the difference between the CCSD(T) and the DFT results, which can be used as a correction term to the DFT values.

Table S2: Vertical formation energies,  $G_f^q$  for  $F^0$  and  $F_s^0$  as obtained from embedded cluster DFT and CCSD(T) calculations, all in eV.

Defect site	Cluster model	PBE	PBE0	B3LYP	CCSD(T)
Terrace	$Mg_5O_5$	6.78	6.53	6.80	6.52
	$Mg_{50}O_{50}$	6.54			
Bulk	$Mg_6O_9$	7.18	7.02	7.37	7.09
	$Mg_6O_9$ (FHI-aims)	7.11	6.99	7.35	
	$Mg_{14}O_{19}$	7.06			

## 2 Extrapolation to dilute limit for periodic calculations

The formation energy of a neutral F center is already converged for a very small supercell of 64 atoms, while the formation energies of the  $F^+$  and the  $F^{2+}$  centers show a strong dependence on  $L$ , the higher the charge state the more pronounced is the effect. The difference in formation energy for a 1728 atom supercell compared to a 1000 atom supercell is still 0.05 eV for the  $F^{2+}$  center. It is generally accepted that the leading contributions to the bulk defect formation energy dependence on the supercell size are the terms  $\sim 1/L$  and  $\sim 1/L^3$ , where  $L$  is the supercell lattice constant. This implies that finite-size scaling according to

$$G_f^{\text{bulk},q}(L, \epsilon_F, \mu_O) = G_f^{\text{bulk},q}(L \rightarrow \infty, \epsilon_F, \mu_O) + \frac{a_1}{L} + \frac{a_2}{L^3} \quad (2.1)$$

leads to the correct formation energy in the dilute limit  $G_f^{\text{bulk},q}(L \rightarrow \infty)$ .

The extrapolation procedure correctly incorporates the effects of atomic relaxation. Calculating supercells containing up to 2000 atoms for the doubly charged vacancies, using PBE exchange-correlation treatment, we get an accuracy of 0.05 eV for the extrapolated values of the formation energies. Vibrational contributions are estimated to be small and therefore neglected.

The defect formation energies calculated with HSE06 for the two smallest supercells (64 and 216 atom cells) lie exactly on the same fitting curve as the PBE formation energies, but shifted by a constant value (Fig. S4). Therefore, in all cases HSE formation energies are calculated for the smallest supercell, and then extrapolated to the dilute limit, where  $1/L \rightarrow 0$ , using a shifted PBE fitting function.

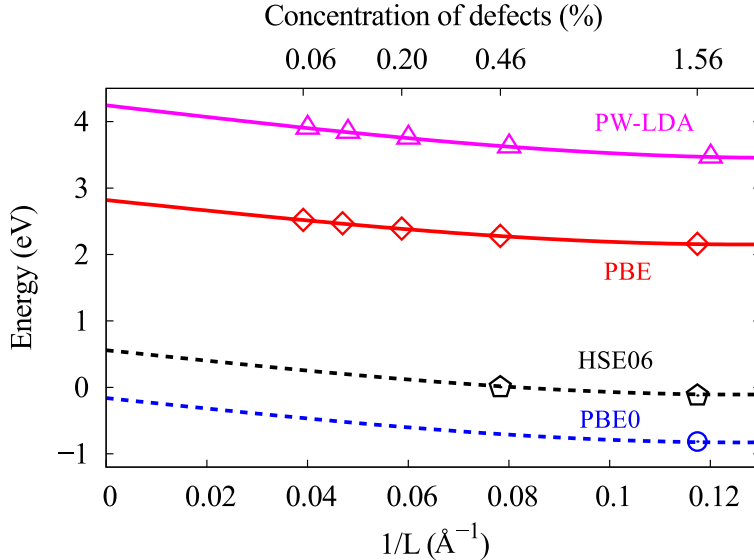


Figure S4: Finite-size scaling for the  $F^{2+}$  center formation energy ( $\epsilon_F = \text{VBM}$ ,  $\mu_O = 1/2 E_{O_2}^{\text{tot}}$ ). Solid lines show fits to  $G_f^{\text{bulk},2}(L) = a_0 + \frac{a_1}{L} + \frac{a_2}{L^3}$  for PW-LDA and PBE formation energies. Formation energies obtained with HSE06 lie on the shifted PBE curve. Accordingly, PBE coefficients  $a_1$  and  $a_2$  are used to extrapolate to isolated defects for all members of the HSE( $\alpha, \omega$ ) functional family.

Although computationally demanding, using the uniform neutralizing background method or the virtual crystal approximation together with extrapolation to the dilute limit is a reliable method for calculating formation energies of charged bulk defects. For charged surface defects, computed using

VCA, the extrapolation is slightly different due to the broken symmetry at the surface. While for bulk supercells, the formation energies were fit to equ. 2.1, where a term proportional to  $\frac{1}{L^2}$  is zero due to symmetry reasons, for the surface defects this term has to be included. The fitting function used is therefore

$$G_f^{\text{surf},q}(L, \epsilon_F, \mu_O) = G_f^{\text{surf},q}(L \rightarrow \infty, \epsilon_F, \mu_O) + \frac{a_1^q}{L} + \frac{a_2^q}{L^2} + \frac{a_3^q}{L^3}. \quad (2.2)$$

Two new aspects have to be taken care of when calculating the extrapolated formation energies for the isolated F centers at the surface. The periodicity of the calculation is three-dimensional, so the slabs are separated by vacuum to remove undesired interactions between repeating slabs. The reference unit cell is neutral, because the compensating charge  $-q$  to the defect charge  $q$  is distributed on the Mg atoms in the slab. Since FHI-aims uses localized basis functions, there is no computational extra-cost when the vacuum region is chosen large. Here, the smallest distance between a defect and its image in  $z$ -direction, perpendicular to the surface, was chosen as 200 Å. Using a slab to model an isolated defect in a semi-infinite system, only makes sense, if convergence of the desired property can be reached with respect to the number of layers  $N_L$  in the slab. The electrostatic energy in the slab depends obviously on  $N_L$  and this leads to different extrapolation curves, as shown for  $F_s^{2+}$  with slabs of  $N_L = 4, 5, 6$  and 7 in Fig. S5. Full relaxation has been performed for all slab systems (using PBE), since also the geometric relaxation convergence and lattice polarizability may vary with  $N_L$ . While a 4 layer slab is not sufficient to obtain an accurate result for the extrapolated formation energy, where  $1/L \rightarrow 0$ , the 5 layer and 6 layer slab models yield the same value.

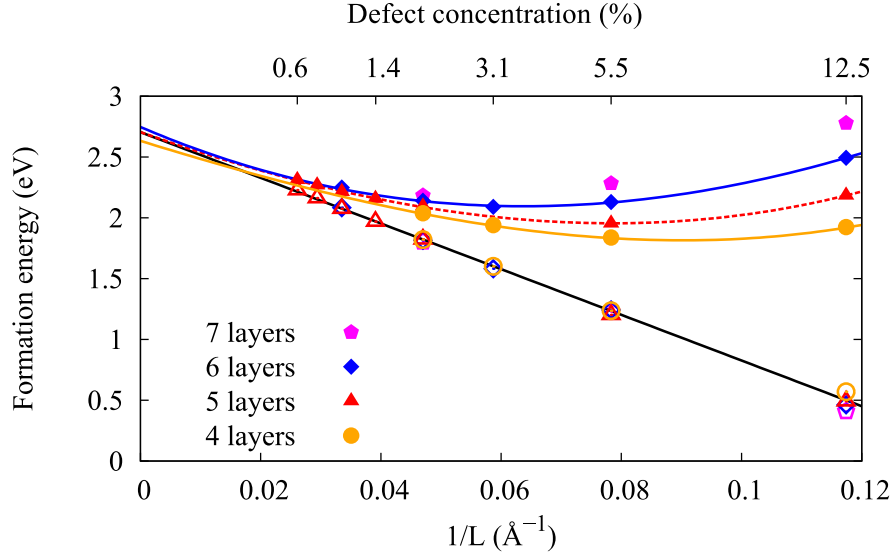


Figure S5: Extrapolation of the  $F_s^{2+}$  formation energy  $\Delta G_f(L)$  (filled symbols, vibrations and dispersion neglected) to infinite supercell size ( $L \rightarrow \infty$ ) for different numbers of layers in the slab, calculated with PBE. The Fermi level is at VBM and  $\mu_O = 1/2 E_{O_2}^{\text{tot}}$ . Open symbols and linear fit (black line) are obtained by subtracting the band bending contribution (Eq. 2.3).

The electrostatic energy that causes the formation energy of charged defects to increase with slab thickness  $d$  is the band bending (see main text). This contribution can be calculated as follows (see chapter 5 below):

$$qE^{\text{SC}} = \frac{q^2 e}{6\epsilon_r \epsilon_0} \frac{d}{L^2} \quad (2.3)$$

where  $e$  is the absolute value of electron charge. Subtracting  $qE^{\text{SC}}$  from the formation energies at every cell size  $G_f^{\text{surf},q}(L)$  removes the term  $\propto 1/L^2$  in the finite-size scaling curve for each slab

thickness. This is shown on the example of the  $F_s^{2+}$  center ( $q = 2$ ) at the MgO (100) terrace in Fig. S5. The term  $\propto 1/L^3$  plays a role only for small  $L$ , so that the remaining linear dependence coincides for slabs with a number of layers  $N_L = 4, 5, 6$  and 7 for all calculated surface charge densities  $\sigma = 2e/L^2$ . The solid black line shows a linear fit, incorporating all calculated formation energies. This linear fit yields the same value for the formation energy of the isolated defect as obtained before for different slab thicknesses using equ. 2.2. The linear term is present due to the electrostatic attraction between the defects and the compensating charge. Thus, equ. 2.2 yields full information on the dependence of the formation energy on defect concentration.

Equ. 2.2 can be generalized to the case when defects in different charge state (+ or 2+) coexist at the surface. First, we rewrite equ. 2.2 in terms of surface charge density  $\sigma_q$  for  $q = 1, 2$  using  $\sigma_q = qe/L^2$ :

$$G_f^{\text{surf},q}(\sigma_q, d) = G_f^{\text{surf},q}(\sigma_q \rightarrow 0) + a_1^q \left( \frac{\sigma_q}{qe} \right)^{\frac{1}{2}} + a_2^q(d) \left( \frac{\sigma_q}{qe} \right) + a_3^q(d) \left( \frac{\sigma_q}{qe} \right)^{\frac{3}{2}}. \quad (2.4)$$

(Vibrational energy contributions to the formation energies are found to be insignificant for this study and therefore neglected.) When defects in both charge states are present at the surface simultaneously, the surface charge density is  $\sigma = \sigma_1 + \sigma_2$ . Since the nature of the second and third terms is purely electrostatic, we apply a mean-field approximation and simply replace  $\sigma_q$  with  $\sigma$  in these terms. The fourth term is more complicated since in addition to higher-order electrostatic effects it also includes geometric relaxation effects. However, also in this term we replace  $\sigma_q$  with  $\sigma$ , which corresponds to averaging the relaxation effects over different defect charge states. This averaging may give a noticeable error only in the specific case of comparable, and at the same time not small ( $> 3\%$ ), concentrations of  $F_s^+$  and  $F_s^{2+}$ . Thus, the dependence of the formation energies on the overall surface charge density  $\sigma$  is given by:

$$G_f^{\text{surf},q}(\sigma, d, \epsilon_F, \mu_O) = G_f^{\text{surf},q}(\sigma \rightarrow 0, \epsilon_F, \mu_O) + a_1^q \left( \frac{\sigma}{qe} \right)^{\frac{1}{2}} + a_2^q(d) \left( \frac{\sigma}{qe} \right) + a_3^q(d) \left( \frac{\sigma}{qe} \right)^{\frac{3}{2}}. \quad (2.5)$$

Note, that  $G_f^{\text{surf},q}(\sigma \rightarrow 0)$  depends on Fermi energy  $\epsilon_F$  and reservoir for oxygen atoms  $\mu_O(T, p_{O_2})$ . The calculated values of  $G_f^{\text{surf},q}(\sigma \rightarrow 0)$  and  $a_i^q$ ,  $i = 1-3$ , for the 5-layer slab as obtained by extrapolation, are summarized in Table S3. The corresponding values, when  $a_2^q$  was extracted from equ. 2.3 are shown in Table S4.

Table S3:  $G_{\text{f}}^{\text{surf},q}(\sigma \rightarrow 0)$  as obtained with HSE06 and coefficients  $a_i^q$ ,  $i = 1-3$  for the 5-layer slab ( $\epsilon_{\text{F}}=\text{VBM}$ ,  $\mu_{\text{O}} = 1/2 E_{\text{O}_2}^{\text{tot}}$ )

q	$G_{\text{f}}^{\text{surf},q}(\sigma \rightarrow 0)(\text{eV})$	$a_1^q(\text{eV}\text{\AA})$	$a_2^q(\text{eV}\text{\AA}^2)$	$a_3^q(\text{eV}\text{\AA}^3)$
0	6.34	0	0	0
1	2.76	-4.93	24.76	42.29
2	0.55	-17.49	80.86	258.11

Table S4:  $G_{\text{f}}^{\text{surf},q}(\sigma \rightarrow 0)$  as obtained with HSE06 and coefficients  $a_i^q$ ,  $i = 1-3$  for the 5-layer slab ( $\epsilon_{\text{F}}=\text{VBM}$ ,  $\mu_{\text{O}} = 1/2 E_{\text{O}_2}^{\text{tot}}$ ), where  $a_2^q$  was obtained from equ. 2.3

q	$G_{\text{f}}^{\text{surf},q}(\sigma \rightarrow 0)(\text{eV})$	$a_1^q(\text{eV}\text{\AA})$	$a_2^q(\text{eV}\text{\AA}^2)$	$a_3^q(\text{eV}\text{\AA}^3)$
0	6.34	0	0	0
1	2.77	-5.30	30.69	14.35
2	0.60	-20.13	122.78	62.93



### 3 Summary of formation energies for F centers in MgO in the dilute limit

Table S5: Formation energies  $G_f^q(\sigma \rightarrow 0)$  (all in eV) of the  $F^0$ ,  $F^+$  and  $F^{2+}$  center in MgO bulk and the  $F_s^0$ ,  $F_s^+$  and  $F_s^{2+}$  center at the MgO (100) surface terrace site, calculated at different levels of exchange-correlation treatment within periodic boundary conditions (pbc) as well as using embedded cluster models (ecm). Periodic calculations and ecm computations with HSE06 have been performed with FHI-aims, while for all other ecm calculations TURBOMOLE was used. The Fermi level is at the VBM, where the VBM with respect to vacuum level was calculated using periodic slab models of the ideal surface. The chemical potential of oxygen is at the oxygen-rich limit where  $\Delta\mu_O = 0$ . Our best numbers are highlighted in boldface.

Method	$F^0$	$F^+$	$F^{2+}$	$F_s^0$	$F_s^+$	$F_s^{2+}$
PBE-pbc	7.09	4.54	2.82	6.48	4.18	2.68
HSE06-pbc	<b>7.04</b>	<b>3.33</b>	<b>0.56</b>	<b>6.34</b>	<b>2.76</b>	<b>0.55</b>
PBE0-pbc	7.07	2.95	-0.16	6.33	2.56	0.12
HSE06-ecm	7.05	-	-	-	-	-
PBE-ecm[ $\Delta$ CCSD(T)]	<b>6.94</b> [-0.09]	-	-	<b>6.49</b> [-0.26]	4.17	2.26
PBE0-ecm[ $\Delta$ CCSD(T)]	<b>6.81</b> [+0.07]	-	-	<b>6.26</b> [-0.01]	2.54	-0.30
B3LYP-ecm[ $\Delta$ CCSD(T)]	<b>7.17</b> [-0.28]	-	-	<b>6.61</b> [-0.28]	3.05	0.13

Table S6: Formation energies  $G_f^{q=0}$  (all in eV) of the neutral  $F_s^0$  center at the MgO (100) surface corner, reverse corner, step and edge, in the O-rich limit, calculated using embedded cluster models. For more information on these defects, see also [3].

Method	Reverse corner	Step	Edge	Corner
HF [4]	-	4.24	-	3.24
LDA [5]	6.76	6.99	-	5.45
PBE	5.94	5.68	5.76	5.13
PBE0	5.69	5.44	5.53	4.89
B3LYP [3]	5.91	5.61	5.78	5.01
B3LYP [2]	-	-	-	4.63

## 4 Valence-band maximum with respect to vacuum level

In the periodic calculations of the MgO (100) surface a vacuum region of  $\approx 200\text{\AA}$  separates repeating 5 layer MgO slabs. The potential in the middle of this vacuum region is the vacuum level  $E_{\text{VAC}}^{\text{Surf}}$  for the surface calculation. To obtain the valence-band maximum (VBM) with respect to vacuum level for the bulk system,  $E_{\text{VBM-VAC}}^{\text{Bulk}}$ , a surface slab calculation is performed with the respective exchange-correlation functional and the difference between  $E_{\text{VAC}}^{\text{Surf}}$  and the 1s core level of Mg in the deepest, bulk-like layer  $E_{\text{core}}^{\text{Surf}}$  is determined. This difference is added to the Mg 1s core level in the bulk system  $E_{\text{core}}^{\text{Bulk}}$  and the resulting bulk vacuum level is subtracted from the bulk VBM  $E_{\text{VBM}}^{\text{Bulk}}$

$$E_{\text{VBM-VAC}}^{\text{Bulk}} = E_{\text{VBM}}^{\text{Bulk}} - \left( E_{\text{core}}^{\text{Bulk}} + (E_{\text{VAC}}^{\text{Surf}} - E_{\text{core}}^{\text{Surf}}) \right). \quad (4.1)$$

## 5 Concentration of surface defects

*P*-type dopants deep in the bulk set the Fermi level to VBM. As described in the main text, the formation energy of charged defects for a surface charge density  $\sigma$  is:

$$G_{\text{f}}^q(\sigma, z^{\text{SC}}(\sigma)) = G_{\text{f}}^q(\sigma, d) - qE^{\text{SC}}(\sigma, d) + qE^{\text{SC}}(\sigma, z^{\text{SC}}), \quad (5.1)$$

where  $G_{\text{f}}^q(\sigma, d)$  is calculated by VCA and is given by equ. 2.5,  $E^{\text{SC}}$  is the band bending contribution, and  $z^{\text{SC}}$  is the thickness of the space-charge layer. For a given concentration of dopants  $N_{\text{D}}$ ,

$$z^{\text{SC}} = \frac{\sigma}{eN_{\text{D}}}. \quad (5.2)$$

At temperature  $T = 0$  K, the above  $z^{\text{SC}}$  minimizes the electrostatic energy of the system under the constraints of constant surface charge density and charge neutrality. At finite  $T$ ,  $z^{\text{SC}}$  has a profile that minimizes the free energy of the system at that  $T$ . We estimated the effect of temperature on  $z^{\text{SC}}$ , and found it to be small at realistic  $T$ ,  $\sigma$ , and  $N_{\text{D}}$ . Therefore, we use equ. 5.2 to calculate  $z^{\text{SC}}$ . The formula for  $E^{\text{SC}}(\sigma, z^{\text{SC}})$  is obtained by integrating the Maxwell equation for a charge density  $\rho(\mathbf{r}) = \delta(z)\sigma - \sigma/z^{\text{SC}}$ :

$$\mathbf{E}_z = \frac{\sigma}{\epsilon_r \epsilon_0} \left( 1 - \frac{z}{z^{\text{SC}}} \right) \mathbf{e}_z, \quad (5.3)$$

where  $\mathbf{E}_z$  is the electric field along the surface normal  $\mathbf{e}_z$ .  $\sigma E^{\text{SC}}(\sigma, z^{\text{SC}})$  is the energy required to take electrons from the surface and distribute them uniformly over the thickness  $z^{\text{SC}}$ , recalculated per defect:

$$\sigma E^{\text{SC}}(\sigma, z^{\text{SC}}) = \frac{1}{2} \int_0^{z^{\text{SC}}} E_z^2 dz = \sigma \frac{\sigma}{6\epsilon_r \epsilon_0} z^{\text{SC}}. \quad (5.4)$$

The potential difference  $\Delta\phi$  due to band bending can be calculated by integrating equ. 5.3:

$$\Delta\phi = -\frac{\sigma}{2\epsilon_r \epsilon_0} z^{\text{SC}} \quad (5.5)$$

The change in Gibbs free energy per unit area upon defect formation is:

$$\Delta g(\eta_0, \eta_1, \eta_2, T, p_{\text{O}_2}, N_{\text{D}}) = \eta_0 G_{\text{f}}^0 + \sum_{q=1}^2 \eta_q G_{\text{f}}^q(\sigma, z^{\text{SC}}(\sigma, N_{\text{D}})) - T \sum_{q=0}^2 s_{\text{conf}}^q(\eta_0, \eta_1, \eta_2), \quad (5.6)$$

where  $\eta_0$ ,  $\eta_1$ , and  $\eta_2$  are concentrations of the surface defects  $F_s^0$ ,  $F_s^+$ , and  $F_s^{2+}$ , respectively, the total surface charge density  $\sigma = e\eta_1 + 2e\eta_2$ , and  $s_{\text{conf}}^q(\eta_0, \eta_1, \eta_2)$  is the configurational entropy per unit area. The configurational entropy accounts for all possible defect arrangements that have the same energy. Due to the screening of the charged defects by the compensating charge, the number of defect arrangements that have significantly different energy relative to the total number of possible arrangements at the surface for fixed  $\eta_0$ ,  $\eta_1$ , and  $\eta_2$  is expected to be small, and is vanishing for small defect concentrations. Equilibrium defect concentrations  $\eta_0$ ,  $\eta_1$ , and  $\eta_2$  can be found by minimizing  $\Delta g$  with respect to these concentrations:

$$\frac{\partial \Delta g}{\partial \eta_q} = G_{\text{f}}^{\text{eff},q}(\sigma, T, p_{\text{O}_2}, N_{\text{D}}, \epsilon_{\text{F}}) - T \frac{\partial \sum_{r=0}^2 s_{\text{conf}}^r(\eta_0, \eta_1, \eta_2)}{\partial \eta_q} = 0. \quad (5.7)$$

Here,

$$G_{\text{f}}^{\text{eff},q}(\sigma, T, p_{\text{O}_2}, N_{\text{D}}, \epsilon_{\text{F}}) = \frac{\partial}{\partial \eta_q} \sum_{r=0}^2 \eta_r G_{\text{f}}^{\text{surf},r}(\sigma, T, p_{\text{O}_2}, N_{\text{D}}, \epsilon_{\text{F}}) \quad (5.8)$$

is an effective formation energy that includes interaction between the defects. The configurational entropy for each type of defect is:

$$s_{\text{conf}}^q = k_{\text{B}} \left( \eta_q^{\text{sites}} \ln \eta_q^{\text{sites}} - \eta_q \ln \eta_q - (\eta_q^{\text{sites}} - \eta_q) \ln (\eta_q^{\text{sites}} - \eta_q) \right), \quad (5.9)$$

where  $\eta_q^{\text{sites}}$  is the surface density of available sites for the given type of defect:

$$\eta_q^{\text{sites}} = \eta^{\text{sites}} - \sum_{i \neq q} \eta_i \quad (5.10)$$

For MgO (100) surface, the surface density of oxygen atoms is  $\eta^{\text{sites}} = 0.11 \cdot 10^{16} \text{ cm}^{-2}$ .

For simplicity, we omit derivation for equilibrium concentrations in the case when all defect charge states are present at the surface. Due to higher formation energies of  $F_s^0$  and  $F_s^+$  compared to  $F_s^{2+}$ ,  $F_s^0$  and  $F_s^+$  concentrations are found to be relatively small, and can be omitted. The  $F_s^{2+}$  concentration,  $\eta_2$ , can then be found from the following equation:

$$G_{\text{f}}^{\text{eff},2}(2e\eta_2, T, p_{\text{O}_2}, N_{\text{D}}) - k_{\text{B}} T \ln \frac{\eta^{\text{sites}} - \eta_2}{\eta_2} = 0. \quad (5.11)$$

This equation can be easily solved numerically. The results are presented in the letter.

## Bibliography

- [1] C. R. A. Catlow, I. D. Faux, and M. J. Norgett, J. Phys. C: Solid State Phys. **9**, 419 (1976)
- [2] P. V. Sushko, A. L. Shluger, and C. A. Catlow, Surf. Sci. **450**, 153 (2000)
- [3] S. Siculo and J. Sauer, J. Phys. Chem. **117**, 8365 (2013)
- [4] G. Pacchioni and P. Pescarmona, Surf. Sci. **412-413**, 657 (1998)
- [5] L. Kantorovich, J. Holender, and M. Gillan, Surf. Sci. **343**, 221 (1995)